

Effect of Heat Treatment on Corrosion Behaviors of Mg-5Y-2Nd-3Sm-0.5Zr Alloys

Yunwei Gui¹, Quanan Li^{1,2,*}, Jun Chen^{1,2}

¹ School of Materials Science and Engineering, Henan University of Science and Technology, Luoyang 471023, China

² Collaborative Innovation Center of Nonferrous Metals, Luoyang 471023, China

*E-mail: liquanan2016@163.com

Received: 11 September 2018 / Accepted: 9 November 2018 / Published: 5 January 2019

The effect of heat treatment on corrosion behaviors of Mg-5Y-2Nd-3Sm-0.5Zr alloy was investigated. The microstructure and precipitates were studied by X-ray diffraction spectroscopy (XRD), scanning electron microscope (SEM) and energy dispersive spectrometer (EDS). The weight loss rate of samples under different conditions was as-cast > T6-6 h > T6-18 h > T4 > T6-12 h. Open circuit potential (OCP) showed that T6-12 h samples have higher positive potentials than other samples. The potential polarization curves showed that the as-cast sample had the highest corrosion current density, while the T6-12 h sample had the lowest one. EIS results showed that heat treatment improved the corrosion resistance of Mg-5Y-2Nd-3Sm-0.5Zr alloy. It was owing to that the heat treatment process reduced the segregation phases in the Mg-5Y-2Nd-3Sm-0.5Zr alloy and improved the uniformity of the alloy structure. The corrosion rate of different samples depended mainly on the second phases, which played a dual role, depending on their quantity and distribution. The presence of the second phases in the alloy will reduce the corrosion resistance, because it can be used as an effective cathode current. On the contrary, the homogeneous and fine second phases can play a good role in preventing the formation and expansion of corrosion.

Keywords: Mg-Y-Nd-Sm alloy; Heat treatment; Precipitated phases; Corrosion resistance; Electrochemistry

1. INTRODUCTION

Magnesium alloys have small density, high specific strength and specific elastic modulus, and the specific stiffness is close to steel and aluminum alloys[1-3]. It is one of the light structural materials widely used at present. In addition, magnesium and its alloys also have excellent properties such as high damping, easy processing and easy recovery[2-4]. It has been widely developed and put into use in many fields such as automobile, aviation, 3C and medical treatment. However, poor corrosion resistance makes it difficult to give full play to its excellent performance[3-8]. Alloying and heat treatment can effectively

improve corrosion resistance of magnesium alloys, and are effective methods to solve the limitations of magnesium alloys[2-10].

WE series magnesium alloys have been widely used as the most successful commercial heat resistant magnesium alloys[4-13]. The main component of the WE series magnesium alloy is Mg-Y-Nd-Zr, in which Zr is a grain refiner, and the strength of these alloys is mainly achieved through the precipitation strengthening of the rare earth elements Y and Nd[7-14]. Compared with the Nd element (3.6 wt%), the Sm element (5.8 wt%) shows a higher maximum solid solubility and precipitation strengthening effect in the magnesium alloy, while the price of Sm is cheaper[8-16]. The aging kinetics and mechanical properties of Mg-Gd-Sm series alloys were studied by Rokhlin L L et al[17]. The results showed that with the increase of Sm content, the aged hardening effect and tensile properties increased[17]. Sm has better solid solution and precipitation strengthening in magnesium alloy than Nd. On this basis, we choose the WE alloy as the base alloy, use the Sm to replace the Nd in the Mg-Y-Nd alloy, and develop a new Mg-5Y-2Nd-3Sm-0.5Zr alloy with lower cost and better performance.

Heat treatment may lead to changes in precipitated phases and redistribution of alloying elements[13-19]. Daquan Li et al have proved that heat treatment affects the precipitates of Mg-4Y-4Sm-0.5Zr alloy[20]. Quanan Li et al reported the effect of Sm on corrosion behaviors of Mg-6Al-1.2Y-0.9Nd alloy which indicated that proper addition of Sm can significantly improve the corrosion-resistance of the alloy[21]. However, the effect of heat treatment on the corrosion properties of Mg-Y-Nd alloys, especially the influence of the newly developed Mg-Y-Nd-Sm series magnesium alloys, is still unclear. In this study, the effect of heat treatment on the corrosion resistance of Mg-5Y-2Nd-3Sm-0.5Zr alloy is investigated. This paper is expected to provide guidance for development of Mg-Y-Nd-Sm based alloys.

2. EXPERIMENTS

2.1 Materials

The experiment was carried out with Mg-5Y-2Nd-3Sm-0.5Zr alloy. The raw materials used for the preparation of the alloy were industrial pure magnesium ($\geq 99.98\%$), Mg-30%Y, Mg-30%Nd, Mg-30%Sm and Mg-30%Zr. All raw materials were dried at 200 °C for 2 hours before smelting, so as to remove moisture from the alloys. Then grinding on the grinder to remove the oxide scale on the alloy surface. The raw materials were then put into a high-purity corundum crucible and smelted in a medium frequency induction furnace. In the melting process, 1% SF₆ + 99% CO₂ (volume fraction) mixed gas was used as protective atmosphere. The alloy was melted in the crucible, heating up to about 750 °C, heat preservation for 5 min, and then pouring the alloy liquid into the metal mold which has been preheated to 250 °C, and the experimental alloy ingot was obtained. The actual composition of the alloy after smelting was measured by ICP: Mg-5.15Y-2.03Nd-3.11Sm-0.45Zr.

The as-cast Mg-5Y-2Nd-3Sm-0.5Zr alloy was cut into 10 mm × 10mm × 10 mm cubic specimen by wire cutting equipment. Solid solution treatment (T4) was carried out for 10 hours at 525 °C and then quenched at hot water with 80 °C. The aging treatment was to keep the samples treated by T4 for 6 hours, 12 hours and 18 hours at 225 °C. Table 1 showed the detailed thermal processes of the samples in

this study.

Table 1. Heat treatment process of the Mg-5Y-2Nd-3Sm-0.5Zr alloys in this paper.

Heat treatment	Homogenizing	Aging	Abbreviated title
As-cast	—	—	As-cast
T4	525 °C, 10 h + 80 °C water quenching	—	T4
T6 (early-aged)	525 °C, 10 h + 80 °C water quenching	225 °C, 6 h + air cooling	T6-6h
T6 (peak-aged)	525 °C, 10 h + 80 °C water quenching	225 °C, 12 h + air cooling	T6-12h
T6 (over-aged)	525 °C, 10 h + 80 °C water quenching	225 °C, 18 h + air cooling	T6-18h

2.2 Experimental procedures and analysis methods

All the surfaces of the samples were ground with 2000 # sandpaper, cleaned and dried. Before the weight loss test, the quality of the samples was measured by an analytical balance of accuracy of ± 0.1 mg, which is m_0 , the unit is mg. The total area of the specimen is S , and the unit is cm^2 . The treated samples were immersed in a mass concentration of 3.5% NaCl solution for immersion test. After the immersion test, the whole bulk sample was analyzed by X ray diffraction. The samples were soaked with chromic acid (200 g/L CrO_3 , 10 g/L AgNO_3) at 90 °C to remove the corrosion products, then cleaned and weighed. The quality was recorded as m . The corrosion rate of the sample is $c = (m_0 - m) / ST$, of which T is the immersion time of sample, unit is hour; unit of c is $\text{mg}/(\text{cm}^2 \cdot \text{h})$.

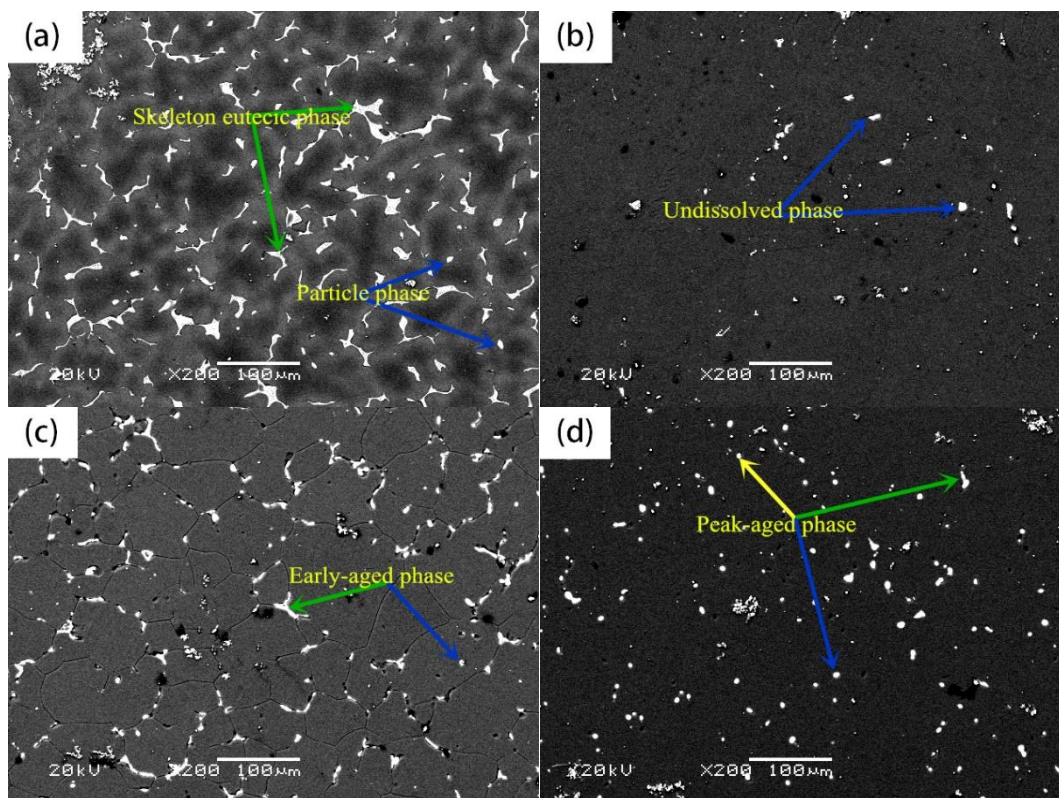
The samples for electrochemical testing were a cube of 10 mm \times 10mm \times 10mm. The samples were polished with 2000 # sandpaper to remove the surface oxide layer, retaining the polished working surface and making it rectangular 10 mm \times 10 mm. Then the samples were bundled with copper wire and sealed with epoxy resin on the non working face. The electrochemical instrument was CHI660E, and the three-electrode system was used for measurement. Among them, the working electrode was Mg-5Y-2Nd-3Sm-0.5Zr, the reference electrode was a saturated potassium chloride electrode, the auxiliary electrode was platinum electrode, and the solution of the electrochemical test was 3.5% NaCl solution. After the open circuit potential (OCP) was stabilized, electrochemical impedance spectroscopy (EIS) and potentiodynamic polarization curves were measured in turn. The frequency sweep range of electrochemical impedance spectroscopy was 100 KHz to 10 MHz (from high to low), and the number of dots was 50. The potential of Tafel polarization curve was ± 0.5 V of OCP, the scanning rate was 0.166 mV/s, and the stride was 0.2 mV.

The microstructure of Mg-5Y-2Nd-3Sm-0.5Zr alloy was characterized by SEM. Observation of corrosion morphology of samples by SEM. After immersion tests, the corrosion products of different samples were calibrated and analyzed by XRD (D8 ADVANCE). The corrosion surface morphology of samples without corrosion products was observed by SEM.

3. RESULTS AND DISCUSSION

3.1 The microstructure of samples

Fig. 1 is the SEM photographs of Mg-5Y-2Nd-3Sm-0.5Zr alloy under different conditions. As shown in Fig. 1 (a), the microstructure of the as-cast alloy consists of α -Mg matrix, a small amount of particle phases and a large number of skeleton eutectic phases distributed along the grain boundaries. After solution treatment, the microstructure of Mg-5Y-2Nd-3Sm-0.5Zr alloy changes obviously. The volume fraction of precipitated phases significantly reduces, the second phase is almost completely dissolved, and the network skeleton of eutectic phase is invisible, leaving only a few particles. And the supersaturated α -Mg matrix is produced in Fig. 1 (b). During the aging treatment process of T6-6 h, second phases precipitates along grain boundary and grain inside, and the main precipitates in Mg-5Y-2Nd-3Sm-0.5Zr alloy microstructure are granular, rod and irregular skeleton, which are irregular in the matrix (as shown in Fig. 1 (c)). With the extension of aging time, the Y, Nd and Sm elements in the matrix gradually precipitate in the form of the second phases and distribute uniformly, as shown in Fig. 1 (d). The second phases are mainly granular and dispersed evenly in the matrix. With the further extension of aging time, fine granular precipitates in the microstructure grow, and some segregation occurs in the microstructure, as shown in Fig. 1 (f).



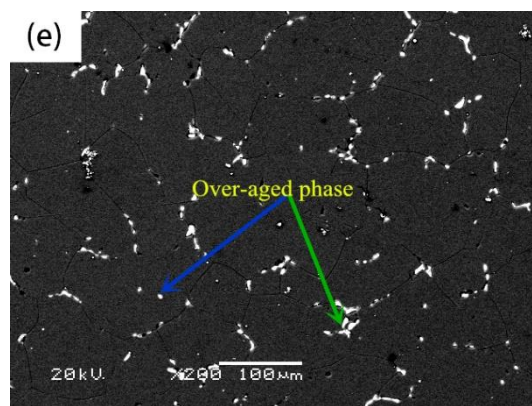


Figure 1. The SEM microstructure pictures of Mg-5Y-2Nd-3Sm-0.5Zr alloys under different heat treatment conditions: (a) as-cast (b) T4 (c) T6-6 h (d) T6-12 h (e) T6-18 h.

The morphology of the second phases of the Mg-5Y-2Nd-3Sm-0.5Zr alloy under different conditions is shown in Fig. 2 (SEM photos) and Table 2 (EDS analysis results).

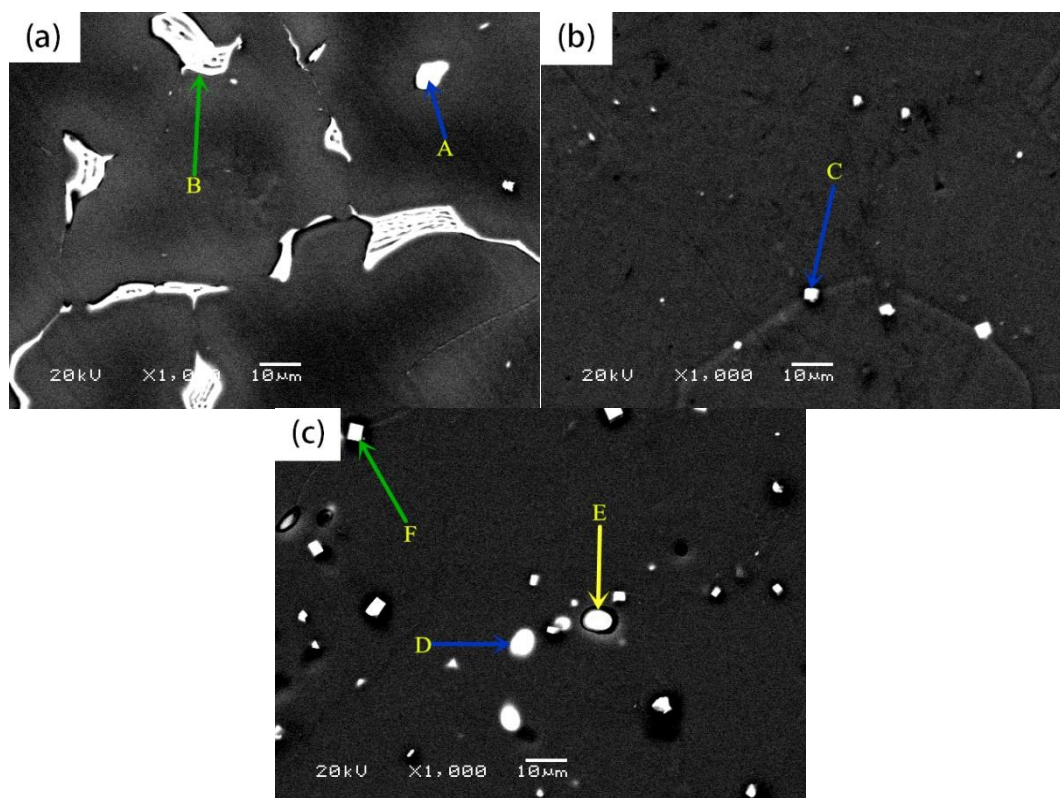


Figure 2. The SEM morphology of different precipitations in Mg-5Y-2Nd-3Sm-0.5Zr alloys under different heat treatment states: (a) as-cast (b) T4 (c) peak-aged (T6-12h).

According to Fig. 2 and Table 2, it can be seen that the A point basically coincide with the content of Mg, Y, Sm and Nd elements in Mg-5Y-2Nd-3Sm-0.5Zr alloy, and the eutectic phases and α -Mg matrix components are equal. However, the mass fraction of Nd and Sm measured at B point is 13.57% and 14.29%, indicating that the irregular skeletal phase at B point is mainly consistent of Nd and Sm. C point contains a small amount of Nd, Sm and Y, indicating that a small amount of Mg-RE compounds are not

dissolved in the α -Mg matrix. The main three phases in the peak-aged state in Fig. 2 (c) are fine and granular. According to the corresponding EDS results, it is found that the D point is mainly the second phase of Sm and Nd, and the E point is a mixed phase containing Sm, Nd, Y, and F point includes mainly Mg-Y phase. According to the previous reports[9-23], the block phase of F point is mainly $Mg_{24}Y_5$.

Table 2. EDS results of the points marked in Figure 2, (wt.%).

Elements (wt.%)	x(Mg)/%	x(Y)/%	x(Nd)/%	x(Sm)/%	x(Zr)/%
Figure 2(a), A	89.53	4.47	1.98	4.02	0.00
Figure 2(a), B	66.36	5.22	13.57	14.29	0.55
Figure 2(b), C	77.12	4.09	4.92	02.86	1.15
Figure 2(c), D	58.67	2.80	20.94	17.58	0.00
Figure 2(c), E	57.14	13.60	13.75	14.43	1.07
Figure 2(c), F	19.37	67.69	3.23	9.09	0.62

The X ray diffraction analysis of alloys at five different states is carried out, as shown in Fig. 3. According to the map calibration, the as-cast Mg-5Y-2Nd-3Sm-0.5Zr alloy is mainly composed of α -Mg, $Mg_{24}Y_5$, $Mg_{41}Sm_5$ and $Mg_{41}Nd_5$ phases. After solution treatment, the second phases in the alloy decrease. With the aging process, the number of diffraction peaks of $Mg_{41}Nd_5$ and $Mg_{41}Sm_5$ increases, the second phases increase, and further increasing with the prolongation of the aging time.

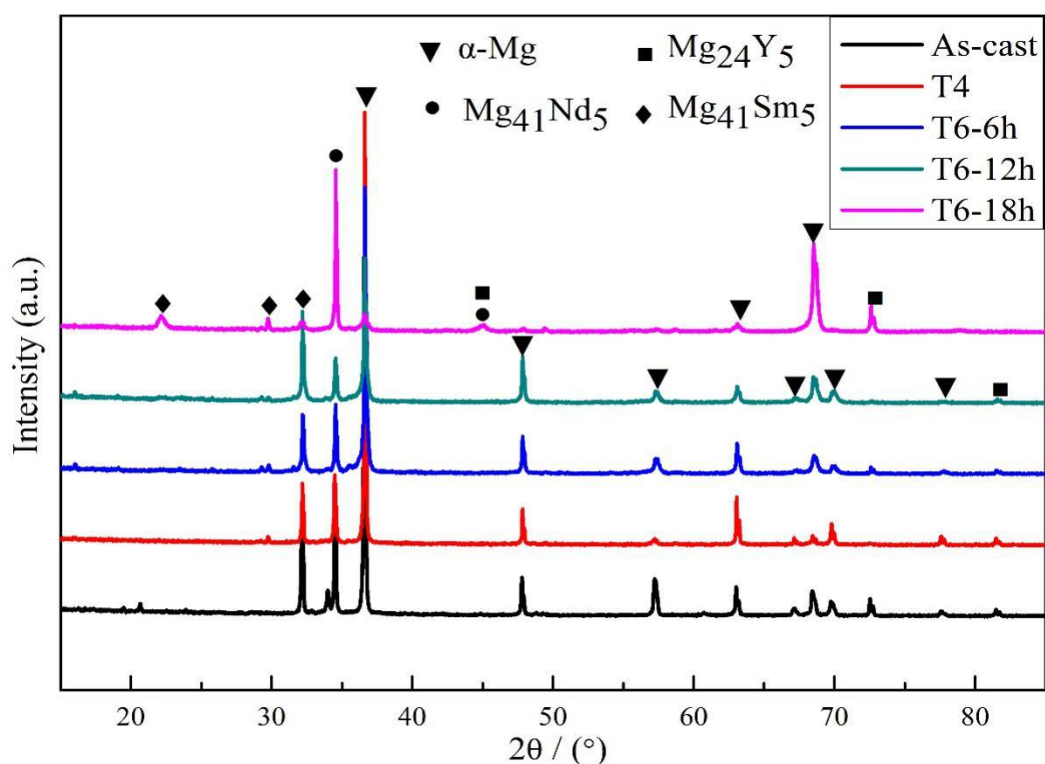


Figure 3. X-ray diffraction patterns of different heat treatment states Mg-5Y-2Nd-3Sm-0.5Zr alloys: as-cast, T4, T6-6 h, T6-12 h, T6-18 h.

3.2 Weight loss rates

Fig. 4 is the average corrosion weight loss rate of Mg-5Y-2Nd-3Sm-0.5Zr alloy under different conditions immersed for 24 h in 3.5% NaCl solution. It can be seen from Fig. 4 that the corrosion loss rate of Mg-5Y-2Nd-3Sm-0.5Zr alloy after solid solution treatment is significantly smaller than that of the as-cast. It shows that solution treatment can effectively improve the corrosion resistance of Mg-5Y-2Nd-3Sm-0.5Zr alloy in NaCl solution. This is mainly due to the uniform surface of the structure and no impurity aggregation on the grain boundaries, so the corrosion resistance of the alloy after solution treatment is higher[11-24]. When the aging time is 12 h at 225 °C, the weight loss rate of the Mg-5Y-2Nd-3Sm-0.5Zr alloy in 3.5% NaCl is lower, which is the most favorable for improving the corrosion resistance of the Mg-5Y-2Nd-3Sm-0.5Zr alloy. This is mainly due to the fine precipitation phase and the dispersion distribution in the matrix, which can inhibit the formation and expansion of corrosion and improve the corrosion resistance of tested alloy[18-25]. Compared with the solid solution, the corrosion weight loss rate of Mg-5Y-2Nd-3Sm-0.5Zr alloy at T6-6 h and T6-18 h did not decrease, but increase. It is indicated that aging treatment does not necessarily enhance the corrosion resistance of the alloy. The improper aging process parameters will weaken the corrosion resistance of the alloy.

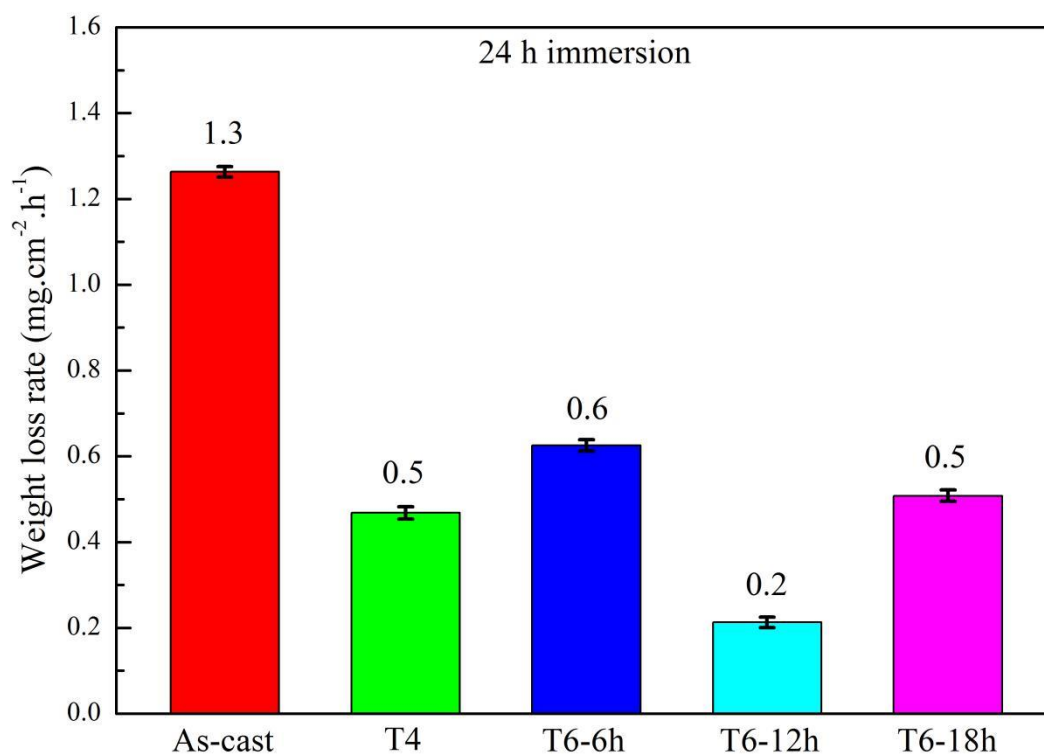


Figure 4. The weight loss rates in 3.5% NaCl solution of Mg-5Y-2Nd-3Sm-0.5Zr alloys in different heat treatment states: as-cast, T4, T6-6 h, T6-12 h, T6-18 h.

3.3 Corrosion products and surface morphologies

In order to further analyse the corrosion products of Mg-5Y-2Nd-3Sm-0.5Zr alloy after immersion in 3.5% NaCl solution, the corrosion products of as-cast, solid solution and peak-aged Mg-

5Y-2Nd-3Sm-0.5Zr alloy are analyzed by X ray diffractometer, as shown in Fig. 5. The main products are $Mg(OH)_2$, $Y(OH)_3$, $Nd(OH)_3$, and $Sm(OH)_3$, in which $Mg(OH)_2$ was the main corrosion product. The corrosion of magnesium matrix occurs in alloy NaCl solution, and the second phases containing rare earth will corrode and dissolve itself. The main reaction is as follows[17-26]:

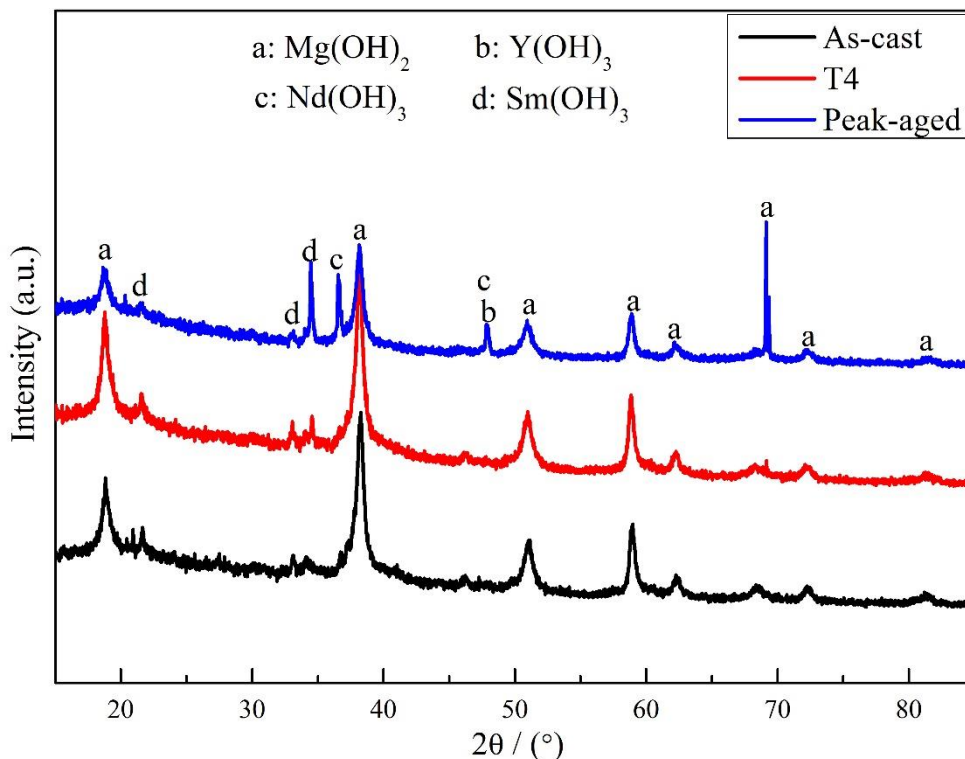
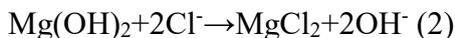
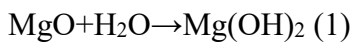


Figure 5. The XRD of corrosion products formed on Mg-5Y-2Nd-3Sm-0.5Zr alloys under different heat treatment conditions: as-cast, T4, peak-aged (T6-12h).

Fig. 6 presents the surface morphology of Mg-5Y-2Nd-3Sm-0.5Zr alloy under different states without corrosion products after immersion in 3.5% NaCl solution. In Fig. 6, the white and coarse face is the corrosion area, and the dark grey and smooth plat is the non-corrosive area. According to the corrosion condition, the as-cast > T6-6 h > T6-18 h > T4 > T6-12 h was ordered, which was in accordance with the calculation results of the corrosion weight loss rate. The corrosion morphology of the as-cast Mg-5Y-2Nd-3Sm-0.5Zr alloy (Fig. 6 (a)) is most serious, and there is a large number of continuous corrosion pitting on the surface. After solution treatment, the corrosion resistance of Mg-5Y-2Nd-3Sm-0.5Zr alloy is increased (Fig. 6 (b)). Fig. 6 (c) shows that T6-6h is similar to as-cast in corrosion morphology, and corrosion is the most serious. Combined with the second phase of the alloy in Fig. 1, this may be related to the coarse skeleton phases in these states. The best corrosion resistance of the alloy surface at 225 °C × 12 h is relatively smooth, and the corrosion pit is small and shallow (as shown in Fig. 6 (d)).

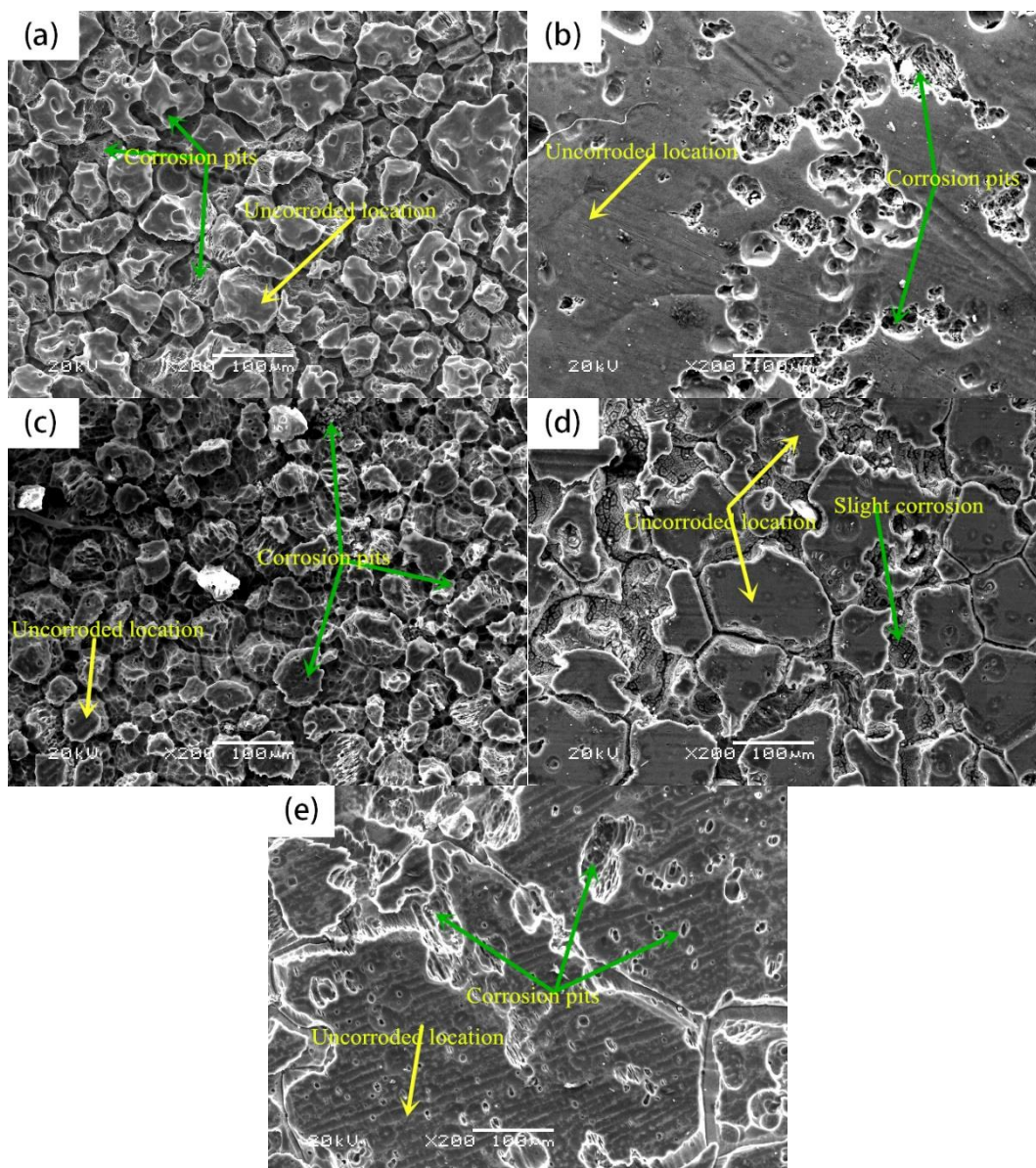


Figure 6. The surface morphologies without corrosion products of different heat treatment Mg-5Y-2Nd-3Sm-0.5Zr samples: (a) as-cast (b) T4 (c) T6-6 h (d) T6-12 h (e) T6-18 h.

3.4 Electrochemical characterizations

Fig. 7 is the open circuit potential curves of Mg-5Y-2Nd-3Sm-0.5Zr alloy with different states in 3.5% NaCl solution. It can be seen from Fig. 7 that the open circuit potentials rise first and then reach equilibrium. We can find that the T6-12h samples have more positive OCP than the other samples, which means that the self-corrosion is lower than as-cast, T4 and other T6 states samples. OCP results show that the order of electrochemical activity can be arranged according to as-cast > T6-6 h > T6-18 h > T4 > T6-12 h.

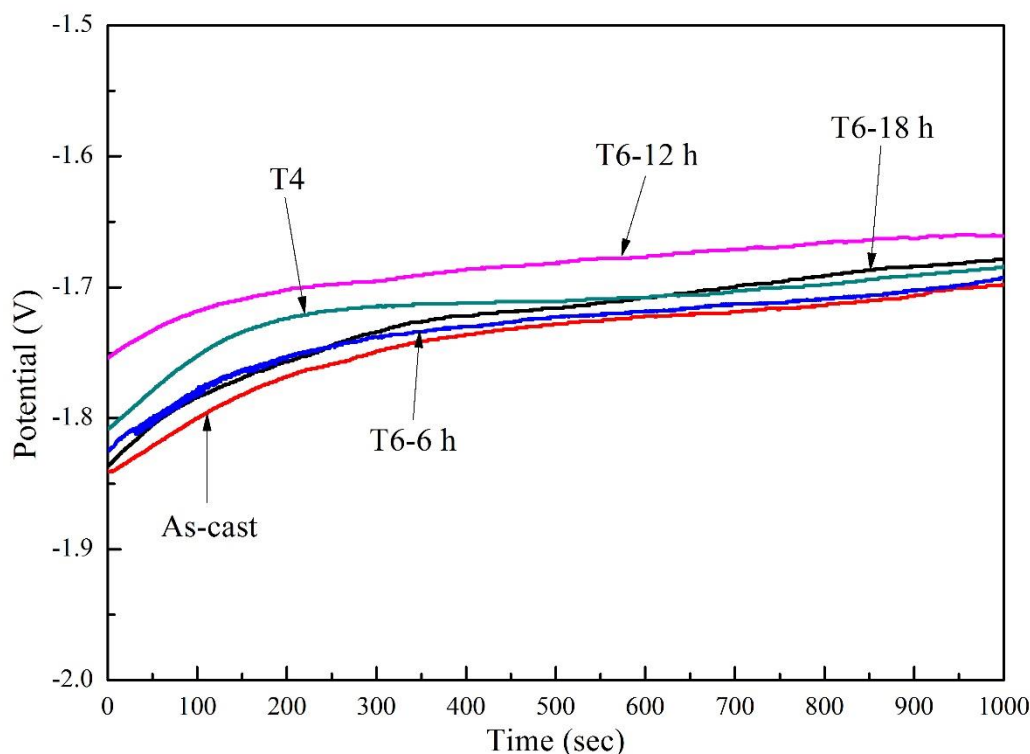


Figure 7. The open circuit potentials (OCP) curves of different heat treatment Mg-5Y-2Nd-3Sm-0.5Zr alloy samples in 3.5% NaCl solution: as-cast, T4, T6-6 h, T6-12 h, T6-18 h.

Fig. 8 shows the effect of heat treatment on the potentiodynamic polarization curves of Mg-5Y-2Nd-3Sm-0.5Zr alloy. The shape of the potentiodynamic polarization curve is similar, showing that the alloy at different states has similar chemical reactions in NaCl solution. The anode branch of potentiodynamic polarization curve can represent the dissolution of Mg-5Y-2Nd-3Sm-0.5Zr alloy matrix, while the cathode branch can represent the hydrogen evolution of the cathode phase in the alloy. During the electrochemical test, it is found that there are bubbles on the surface of the working electrode magnesium alloy because of the negative difference effect. From Fig. 8, it can be seen that the current density of the anode branch changes rapidly and the slope of the curve is greater than the slope of the cathodic branch curve, indicating that the corrosion reaction of the Mg-5Y-2Nd-3Sm-0.5Zr alloy in the 3.5% NaCl solution is cathodic. According to the Tafel formula[16-28]:

$$\Delta E_k = -B_k \lg(i_k / i_c) \quad (3)$$

The corrosion potential E_{corr} is extrapolated in the Tafel area, and the corrosion current density I_{corr} is obtained. The result is shown in Table 3. As shown in Table 3, the self-corrosion potential of Mg-5Y-2Nd-3Sm-0.5Zr alloy in solid solution state and aging state is positively shifted to that of as-cast alloy. It shows that the corrosion tendency of Mg-5Y-2Nd-3Sm-0.5Zr alloy decreases after heat treatment. The corrosion current density of heat treated alloy is lower than that of as-cast, and reaches the lowest at T6-12h. The corrosion resistance of Mg-5Y-2Nd-3Sm-0.5Zr alloy samples is arranged as follows: as-cast > T6-6 h > T6-18 h > T4 > T6-12 h. This is consistent with the corrosion rate of the five alloys tested before. As shown in Table 3, when the corrosion resistance of an alloy is increased or a corrosion inhibitor is added, the Tafel slopes of the anode and cathode are larger. By comparison, the B_c and B_a of the T6-12 h Mg-5Y-2Nd-3Sm-0.5Zr alloy are significantly greater than those of the other stated

alloys. In summary, the T6-12 h Mg-5Y-2Nd-3Sm-0.5Zr alloy has the best corrosion resistance of the alloys tested.

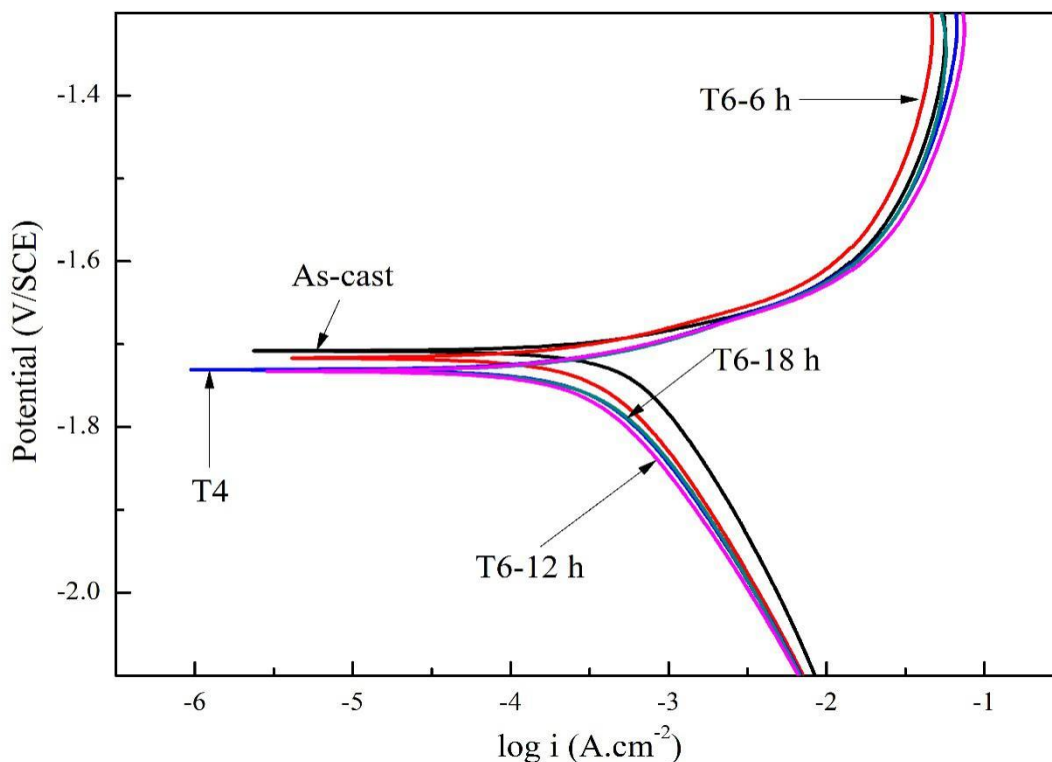


Figure 8. Potentiodynamic polarization curves of Mg-5Y-2Nd-3Sm-0.5Zr alloy with different heat treatments: as-cast, T4, T6-6 h, T6-12 h, T6-18 h.

Table 3. Specific values for Mg-5Y-2Nd-3Sm-0.5Zr alloy with different heat treatments derived from potentiodynamic polarization curves.

Samples	B_a (mV/decade)	B_c (mV/decade)	I_{corr} ($A.cm^{-2}$)	E_{corr} (V)
as-cast	80	40	9.96×10^{-4}	-1.70
T4	122	47	3.74×10^{-4}	-1.73
T6-6 h	100	46	4.48×10^{-4}	-1.71
T6-12 h	128	48	3.11×10^{-4}	-1.73
T6-18 h	123	47	3.85×10^{-4}	-1.73

The electrochemical impedance spectroscopy of Mg-5Y-2Nd-3Sm-0.5Zr alloy with different states in 3.5%NaCl solution is shown Fig. 9. It can be found that heat treatment has no effect on the electrochemical process type of Mg-5Y-2Nd-3Sm-0.5Zr alloy in NaCl solution, but only changes the intensity of each electrochemical reaction. The corrosion resistance of the specimen is better if the radius of the half arc is larger. The specimens are sequentially arranged according to the corrosion resistance from large to small: as-cast > T6-6 h > T6-18 h > T4 > T6-12 h. In addition, it can be seen that there is a resistance arc at the high frequency section of the impedance spectrum, the inductance arc appears in the low frequency section, the emergence of the inductance arc shows the presence of hole erosion, the existence of negative difference effect and the process of the desorption of corrosion products.

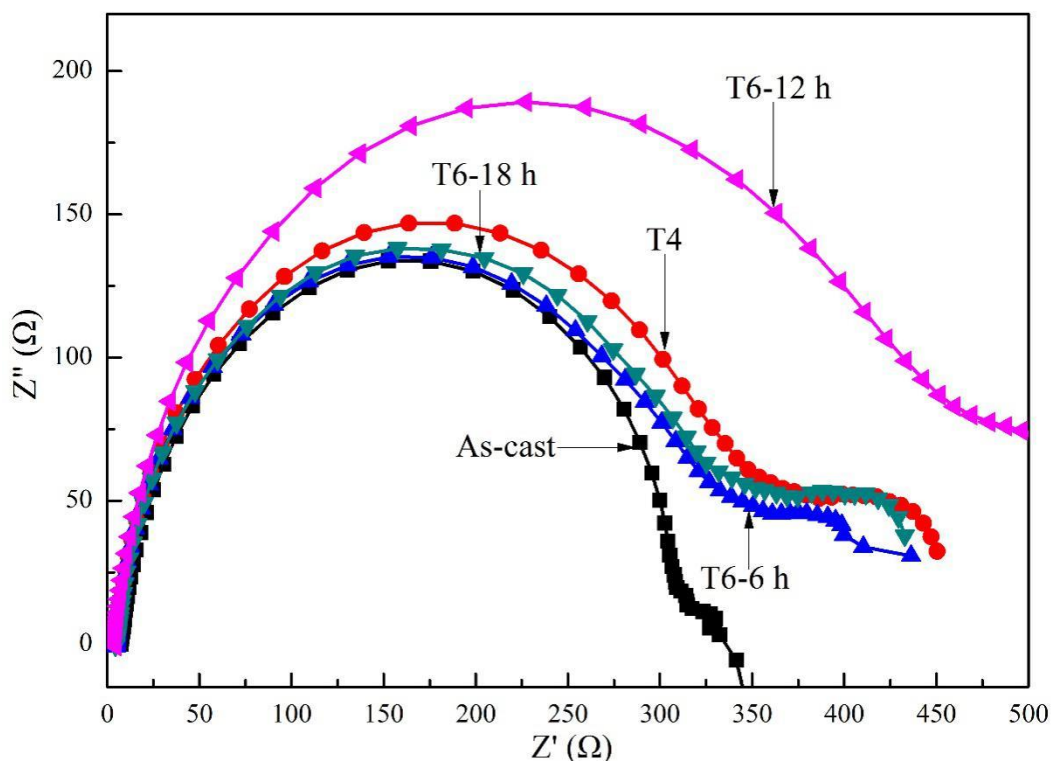


Figure 9. EIS spectra of Mg-5Y-2Nd-3Sm-0.5Zr alloy with different heat treatments: as-cast, T4, T6-6 h, T6-12 h, T6-18 h.

Based on the shape of Nyquist and Bode plots, the equivalent circuit is shown in Figure 10, where R_s is the solution resistance, R_t is the charge transfer resistance, CPE is the constant phase angle element. Table 4 shows the equivalent circuit parameters for the experimental alloys after software fitting. Analysis of the data in Table 4 shows that the R_s values for all the alloys are very small, indicating that the solution resistance has little effect on the experimental process and can be ignored. The R_t of T6-12 h Mg-5Y-2Nd-3Sm-0.5Zr alloy is greatly improved compared with other alloys, while its CPE is significantly reduced. T6-12 h Mg-5Y-2Nd-3Sm-0.5Zr alloy also has a high inductive value, indicating that proper heat treatment can effectively improve the surface condition of the Mg-Y-Nd-Sm alloy, reduces the corrosion tendency of the alloy and hinders the transfer of charge at the interface between the electrode and the electrolyte solution, thereby hindering the progress of the electrode process and improving the corrosion resistance of the alloy.

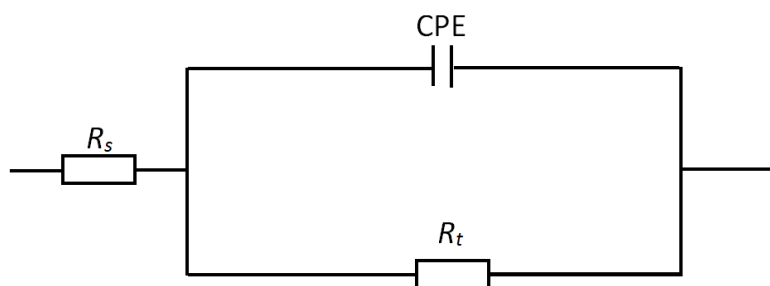


Figure 10. Equivalent circuit of EIS for the Mg-5Y-2Nd-3Sm-0.5Zr alloy with different heat treatments: as-cast, T4, T6-6 h, T6-12 h, T6-18 h.

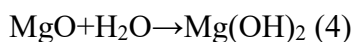
Table 4. Fitting results of the EIS of the Mg-5Y-2Nd-3Sm-0.5Zr alloy with different heat treatments: as-cast, T4, T6-6 h, T6-12 h, T6-18 h.

Samples	$R_s/$ $\Omega \cdot \text{cm}^2$	$CPE/$ $\times 10^{-5} \mu\text{F} \cdot \text{cm}^{-2}$	n	$R_t/$ $\Omega \cdot \text{cm}^2$
as-cast	4.60	2.84	0.907	315.0
T4	4.77	2.26	0.901	388.7
T6-6 h	4.30	2.45	0.896	360.0
T6-12 h	4.54	1.96	0.905	510.3
T6-18 h	4.50	2.44	0.907	376.2

3.5 Corrosion mechanism

3.5.1 Corrosion mechanism of T4 Mg-5Y-2Nd-3Sm-0.5Zr

The corrosion principle diagram of T4 Mg-5Y-2Nd-3Sm-0.5Zr shown in Fig. 10 is established. The corrosion process of T4 Mg-5Y-2Nd-3Sm-0.5Zr alloy is as follows[14-28]: The alloy will form a MgO film in air, and the standard electrode potential of MgO is +1 V. When the magnesium alloy is immersed in the NaCl solution, the oxidation film has a certain corrosion resistance in the position of the oxide film protection, which protects the magnesium matrix, but the protective effect is weak. The oxide film gradually dissolves, and the reaction (4) shows[16-29]:



In NaCl solution, the Cl^- adsorbed on the surface of the material can convert part of the $\text{Mg}(\text{OH})_2$ into the water soluble MgCl_2 , breaks the oxide film on the surface of the magnesium alloy and loses the protection of the matrix. Therefore, the magnesium matrix is directly exposed to NaCl solution, and its reaction is shown in formula (5-8)[19-29]:



The α -Mg matrix is dissolved as an anode, resulting in corrosion producing $\text{Mg}(\text{OH})_2$, and NaCl solution further enters the corrosion pits. Cl^- will continue to convert it into soluble MgCl_2 , so that the magnesium matrix is re-exposed to the corrosive medium. Thus, the pit deepens and the size increases, resulting in localized corrosion and even total corrosion. In the position of no oxide film protection, the alloy matrix is directly contacted with the NaCl solution, and the dissolution of magnesium and the reduction of water are shown, as indicated by the formula (5-8). It is easy to gather the second phase and impurity in the grain boundary, which is the sensitive area of corrosion. Pitting is easy to extend and extend at the grain boundary. On the surface of Mg-5Y-2Nd-3Sm-0.5Zr alloy, the corrosion product membrane is accumulated. As the corrosion increases, the film of the corrosion product falls off and is accompanied by corrosion and exfoliation of the matrix material[21-30].

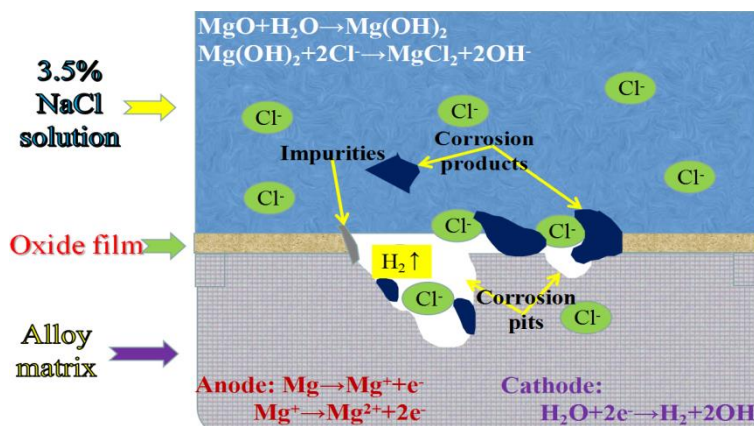


Figure 11. Schematic diagram of the corrosion of T4 state Mg-5Y-2Nd-3Sm-0.5Zr alloy in NaCl solution.

3.5.2 Corrosion mechanism of peak-aged (T6-12h) state Mg-5Y-2Nd-3Sm-0.5Zr

The corrosion principle diagram of T6 Mg-5Y-2Nd-3Sm-0.5Zr shown in Fig. 11 is established. The difference between the schematic diagram of T4 and T6 shown in Fig. 10 is that a lot of second phases (red particles in Fig. 11) precipitated in the aging alloys. Whether the precipitated particles play an important role in improving the corrosion resistance of alloys is mainly related to the quantity, morphology and distribution of precipitates. When the number of precipitates is large, the particles are fine and dispersion distributed in the matrix, the corrosion resistance of the alloy will be improved because of the better corrosion resistance of the precipitated phase and the dispersion distribution on the matrix around the corrosion pit. When the number of precipitates is less, the particle size is larger and the segregation is distributed in the matrix, the electric potential of the rare earth compounds is more positive compared with the α -Mg matrix, so it is easy to form the galvanic corrosion, which aggravates the corrosion rate of the magnesium alloy, so it will weaken the corrosion resistance of the magnesium alloy[13-30].

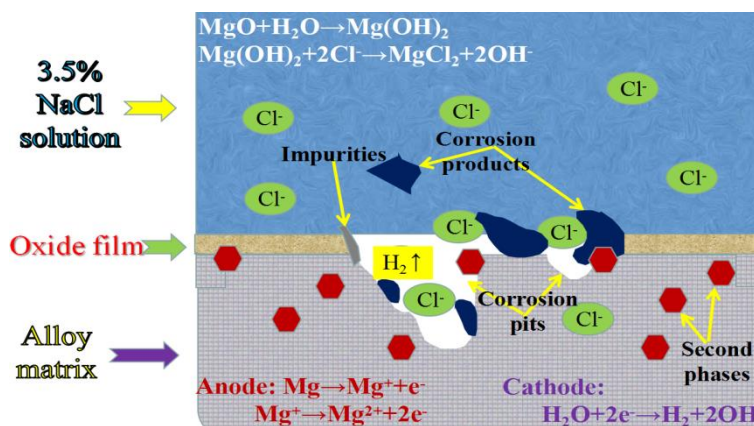


Figure 12. Schematic diagram of the corrosion of peak-aged (T6-12h) state Mg-5Y-2Nd-3Sm-0.5Zr alloy in NaCl solution.

4. CONCLUSION

(1) The microstructure of Mg-5Y-2Nd-3Sm-0.5Zr alloy in different states was mainly composed of α -Mg, Mg₂₄Y₅, Mg₄₁Sm₅ and Mg₄₁Nd₅ phases. After solution treatment, the eutectic phase almost completely dissolved into the matrix. With the extension of aging time, the volume fraction of Mg₄₁Sm₅ and Mg₄₁Nd₅ increased.

(2) The weight loss rate of as-cast sample is highest, while T6-12 h sample is lowest. The electrochemical corrosion activity of different samples can be arranged according to as-cast > T6-6 h > T6-18 h > T4 > T6-12 h. Heat treatment can effectively improve the corrosion resistance of Mg-5Y-2Nd-3Sm-0.5Zr alloy.

(3) The corrosion resistance enhancement of Mg-5Y-2Nd-3Sm-0.5Zr alloy by heat treatment mainly owes to the following two aspects: in the T4 state, the skeletal structure is completely dissolved in the matrix, the surface of the tissue is uniform and without aggregated impurities. Under the peak-aged state (T6-12h), the precipitated phase in the alloy is fine and uniformly distributed in the matrix, which can prevent corrosion and improve the corrosion resistance of Mg-5Y-2Nd-3Sm-0.5Zr alloy.

(4) The results show that the microstructure and precipitates of Mg-5Y-2Nd-3Sm-0.5Zr alloy play an important role. It shows that the corrosion resistance of Mg-5Y-2Nd-3Sm-0.5Zr alloy can be changed by heat treatment.

ACKNOWLEDGEMENTS

This work was supported by the National Natural Science Foundation of China (Nos 51571084 and 51171059), and Henan Province Key Scientific and Technological Projects (Nos 152102210072).

CONFLICTS OF INTEREST

We declare that we do not have any commercial or associative interest that represents a conflict of interest in connection with the work submitted.

References

1. Q.A. Li, X.F. Li, Q. Zhang and J. Chen, *Rare Metals*, 29 (2010) 557.
2. Y. Zhang, C. Yan, F. Wang and W. Li, *Corros. Sci.*, 47 (2005) 2816.
3. J.F. Nie, B.C. Muddle, *Acta. Mater.*, 48 (2000) 1691.
4. S.J. Xia, R. Yue, R.G. Rateick and V.I. Birss, *J. Electrochem. Soc.*, 151 (2004) 179.
5. G.L. Song, A. Atrens, *Adv. Eng. Mater.*, 1(1999) 11.
6. J. Li, Q. Jiang, H. Sun and Y. Li, *Corros. Sci.*, 111 (2016) 288.
7. W.L. Ren, Q.A. Li, J.H. Li, K.J. Li and X.Y. Zhang, *China Foundry*, 117 (2010) 262.
8. J. Chen, Q.A. Li, J.H. Li, X.F. Li, K.J. Li and X.Y. Zhang, *China Foundry*, 6 (2009) 124.
9. K.J. Li, Q.A. Li, X.T. Jing, J. Chen, X.Y. Zhang and Q. Zhang, *Scripta. Mater.*, 60 (2009) 1101.
10. L.L. Rokhlin, N.I. Nikitina, *Phys. Met. Metallogr.*, 82 (1996) 113.
11. H.R.J. Nadooshan, W.C. Liu, G.H. Wu, Y. Rao, C.X. Zhou, S.P. He, W.J. Ding and R. Mahmudi, *Mat. Sci. Eng. A-Struct.*, 615 (2014) 79.
12. B.L. Mordike, T. Ebert, *Mat. Sci. Eng. A-Struct.*, 302 (2001) 37.
13. C.Y. Su, D.J. Li, A.A. Luo, T. Ying and X.Q. Zeng, *J. Alloy. Compd.*, 747 (2018) 431.
14. Y. Fan, G. Wu, H. Gao, G. Li and C. Zhai, *J. Mater. Sci.*, 41 (2006) 409.

15. Y. Song, D. Shan, R. Chen and E.H. Han, *Corros. Sci.*, 52 (2010) 1830.
16. S. Pawar, T.J.A. Slater, T.L. Burnett, X. Zhou, G.M. Scamans, Z. Fan, G.E. Thompson, P.J. Withers, *Acta. Mater.*, 133 (2017) 90.
17. L.L. Rokhlin, N.I. Nikitina, *Phys. Met. Metallogr.*, 82 (1996) 113.
18. H. Qiu, H. Yan and Z. Hu, *J. Alloy. Compd.*, 567 (2013) 77.
19. J.D. Robson, S.J. Haigh, B. Davis and D. Griffiths, *Metall. Mater. Trans. A*, 47 (2016) 522.
20. D.Q. Li, Q.D. Wang and W.J. Ding, *Mat. Sci. Eng. A-Struct.*, 448 (2007) 165.
21. Q.A. Li, X.F. Li, Q. Zhang and J. Chen, *Rare. Metals*, 29 (2010) 557.
22. E. Aghion, B. Bronfin, F.V. Buch, S. Schumann and H. Friedrich, *JOM.*, 55 (2003) 30.
23. L. Shi, D.O. Northwood, *Acta. Metall. Sin.*, 42 (1994) 871.
24. D.Q. Li, Q.D. Wang and W.J. Ding, *Mat. Sci. Eng. A-Struct.*, 448 (2007) 165.
25. S.W. Nam, W.T. Kim, D.H. Kim and T.S. Kim, *Met. Mater. Int.*, 19 (2013) 205.
26. B.J. Wang, D.K. Xu, J.H. Dong, W. Ke, *Scr. Mater.*, 88 (2014) 5.
27. R. Arrabal, A. Pardo, M.C. Merino, M. Mohedano and P. Casajús, *Corros. Sci.*, 55 (2012) 301.
28. M. Sun, G. Wu, W. Wang and W. Ding, *Mat. Sci. Eng. A-Struct.*, 523 (2009) 145.
29. Y.W. Gui, Q.A. Li and J. Chen, *Mater. Res. Express*, 5 (2018) 7.
30. O. Zheng, J.P. Zhou, D.S. Zhao, J.B. Wang and R.H. Wang, *Scripta. Mater.*, 60 (2009) 791.

© 2019 The Authors. Published by ESG (www.electrochemsci.org). This article is an open access article distributed under the terms and conditions of the Creative Commons Attribution license (<http://creativecommons.org/licenses/by/4.0/>).